Loss of Rb proteins causes genomic instability in the absence of mitogenic signaling

Tanja van Harn, Floris Foijer, Marcel van Vugt, et al.

Genes Dev. published online June 15, 2010
Access the most recent version at doi:10.1101/gad.580710

Loss of Rb proteins causes genomic instability in the absence of mitogenic signaling

Tanja van Harn,[1,5] Floris Foijer,[1,2,5] Marcel van Vugt,[3] Ruby Banerjee,[2] Fentang Yang,[2] Anneke Oostra,[4] Hans Joenje,[4] and Hein te Riele[1,6]

[1]Division of Molecular Biology, The Netherlands Cancer Institute, Amsterdam 1066 CX, The Netherlands; [2]Wellcome Trust Genome Campus, Wellcome Trust Sanger Institute, Cambridge CB10 1SA, United Kingdom; [3]Department of Medical Oncology, Groningen Medical Centre, Groningen 9713 GZ, The Netherlands; [4]Department of Clinical Genetics, VU University Medical Center, Amsterdam 1081 BT, The Netherlands

Loss of G1/S control is a hallmark of cancer, and is often caused by inactivation of the retinoblastoma pathway. However, mouse embryonic fibroblasts lacking the retinoblastoma genes *RB1*, *p107*, and *p130* (TKO MEFs) are still subject to cell cycle control: Upon mitogen deprivation, they enter and complete S phase, but then firmly arrest in G2. We now show that G2-arrested TKO MEFs have accumulated DNA damage. Upon mitogen readdition, cells resume proliferation, although only part of the damage is repaired. As a result, mitotic cells show chromatid breaks and chromatid cohesion defects. These aberrations lead to aneuploidy in the descendent cell population. Thus, our results demonstrate that unfavorable growth conditions can cause genomic instability in cells lacking G1/S control. This mechanism may allow premalignant tumor cells to acquire additional genetic alterations that promote tumorigenesis.

[*Keywords*: Cell cycle; DNA damage; Rb; genomic instability; sister chromatid cohesion]

Supplemental material is available at http://www.genesdev.org.

Received February 17, 2010; revised version accepted May 4, 2010.

Cancer cells have successively acquired multiple genetic and/or epigenetic alterations that permit unrestrained proliferation. The G1 checkpoint, which is an important barrier to proliferation under growth inhibitory conditions, is frequently mutated in human tumors by various perturbations in the retinoblastoma tumor suppressor (Rb) pathway (Malumbres and Barbacid 2001). Loss of function of the *RB1* gene is the initiator event in retinoblastoma, a pediatric cancer of the eye (Corson and Gallie 2007; Dimaras et al. 2008). Additionally, inactivation of *RB1* was found in various other tumors, like sporadic breast, bladder, prostate, and small-cell lung carcinoma. Abrogation of the G1 checkpoint can also occur by genetic alteration of upstream regulators of the Rb pathway. Amplification of *Cyclin D1* was found in breast, esophagus, and head and neck cancer, and loss of $p16^{INK4A}$ function was observed in melanoma and pancreatic and bladder carcinomas (Malumbres and Barbacid 2001). Moreover, human papillomavirus (HPV) can initiate cervical carcinoma and squamous cell carcinoma of the head and neck by expression of the E7 oncoprotein that inactivates the protein retinoblastoma (pRB) (Doorbar 2006; Perez-Ordonez et al. 2006).

[5]These authors contributed equally to this work.
[6]Corresponding author.
E-MAIL h.t.riele@nki.nl; FAX 31-20-6691383.
Article published online ahead of print. Article and publication date are online at http://www.genesdev.org/cgi/doi/10.1101/gad.580710.

Besides loss of cell cycle control mechanisms, genomic instability manifested by aneuploidy and chromosomal rearrangements is another hallmark of solid tumors (Marx 2002) and has also been observed in retinoblastomas (Dimaras et al. 2008). Genomic instability may be due to defects in genome maintenance mechanisms by loss, mutation, or epigenetic silencing of genes encoding DNA repair enzymes and checkpoint proteins (Harper and Elledge 2007). However, it has also been suggested that interference with pRB function could promote polyploidy, aberrations in chromosome number, or micronuclei formation (Zheng et al. 2002; Hernando et al. 2004; Gonzalo et al. 2005; Mayhew et al. 2005; Iovino et al. 2006; Srinivasan et al. 2007; Amato et al. 2009). How these alterations originate in pRB-depleted cells is not entirely understood. It has been suggested that DNA double-strand breaks (DSBs) are not repaired properly in pRB-depleted cells. S-phase cells exposed to genotoxic stress slow down replication fork progression to suppress the formation of DSBs (Bosco et al. 2004). This process required dephosphorylation of pRB (Knudsen et al. 2000), and therefore the inability of pRB-defective cells to decelerate S-phase progression could promote DNA damage. Furthermore, pRB deficiency was also shown to attenuate the DNA damage-induced G2 checkpoint due to the up-regulation of many genes required for G2/M progression (Hernando et al. 2004; Jackson et al. 2005; Eguchi et al. 2007). These imperfections

in S and G2 checkpoints in pRB-defective cells may impede efficient DNA damage repair and cause aberrant chromosome segregation during mitosis. As a result, various other genes that could promote tumorigenesis may become abnormally expressed. Thus, loss of pRB function that abrogates the G1 checkpoint may also induce genomic instability and accelerate tumor development.

In cultured cells, depletion of mitogens results in G1 arrest. This arrest is established by inhibition of cyclin–CDK activity (Cyclin D–CDK4/6 complexes), resulting in hypophosphorylation of the Rb proteins, which, besides pRB, compromise p107 and p130. Hypophosphorylated Rb proteins can sequester E2F transcription factors and, by recruiting chromatin modifiers like HDACs, DNMT1, HP1A, and Suv39H1, inhibit the transcription of E2F target genes required for S-phase progression (Burkhart and Sage 2008). The G1 arrest critically depends on the Rb proteins, since complete disruption of the genes encoding pRB, p130, and p107 in mouse embryonic fibroblasts (hereafter referred to as TKO MEFs) abrogated the capacity of these cells to arrest in the G1 phase of the cell cycle (Dannenberg et al. 2000; Sage et al. 2000). However, TKO MEFs were not refractory to mitogen deprivation. Although Rb proteins contribute to the G2 arrest in response to DNA damage (Jackson et al. 2005; Eguchi et al. 2007), we found that mitogen deprivation of TKO MEFs in which the apoptotic response was suppressed by overexpression of the anti-apoptotic protein Bcl2 caused a robust G2 arrest (Foijer et al. 2005). This cell cycle block was accomplished by up-regulation of the cyclin-dependent kinase inhibitors (CKIs) $p27^{Kip1}$ and $p21^{Cip1}$, which were found to bind to and inactivate the cyclin–CDK complexes that are required for G2/M progression.

The accumulation of $p27^{Kip1}$ most likely resulted from down-regulation of PI-3 kinase activity upon mitogen deprivation (Foijer et al. 2008), which activates the Forkhead transcription factors stimulating the transcription of $p27^{Kip1}$ (Medema et al. 2000). However, we also observed up-regulation of $p21^{Cip1}$. Since $p21^{Cip1}$ accumulation in mitogen-starved TKO MEFs was shown to be dependent on ATM/ATR kinase activity and the presence of p53 (Foijer et al. 2005), we wondered whether the up-regulation of $p21^{Cip1}$ was due to the presence of DNA damage. In the present study, we show that mitogen-starved, G2-arrested TKO-Bcl2 MEFs had accumulated many DSBs that, upon restimulation of cells by mitogen addition, were not completely repaired. In addition, chromosomes showed severe loss of centromeric cohesion. These phenomena may be responsible for copy number alterations (CNAs) that were frequently found in descendent cell clones.

Results

The DNA damage response (DDR) delays cell cycle re-entry of G2-arrested TKO-Bcl2 MEFs

TKO-Bcl2 MEFs that had arrested in G2 by 7 d of mitogen deprivation (Fig. 1A, right panel) had accumulated high levels of the CKIs $p27^{Kip1}$ and $p21^{Cip1}$(Foijer et al. 2005). These cells were able to re-enter the cell cycle by readdition of 10% fetal calf serum (FCS), but, interestingly, serum readdition did not result in decreased $p21^{Cip1}$ protein levels (Foijer et al. 2005) and caused an up-regulation of DDR genes (Foijer et al. 2008). We therefore speculated that serum-starved TKO-Bcl2 MEFs have accumulated DNA damage. Such damage would activate the DDR, which results in the recruitment of ATM and phosphorylation of the histone variant H2AX (γ-H2AX) (Harper and Elledge 2007). To obtain evidence for activation of the DDR, we studied the rate of cell cycle re-entry upon serum readdition in the presence of either caffeine, an inhibitor of the ATM/ATR kinases (Sarkaria et al. 1999), or UCN-01, an inhibitor of the downstream kinase CHK1 (Graves et al. 2000). Figure 1, B and C, shows that, upon serum readdition, the appearance of mitotic cells was accelerated by caffeine; the appearance of mitotic TKO-Bcl2 MEFs after stimulation with only 10% FCS peaked 6 h later than after stimulation with 10% FCS in the presence of caffeine. Also, UCN-01 accelerated mitotic entry of serum-restimulated TKO-Bcl2 MEFs (Supplemental Fig. S1). Furthermore, we found that restimulation in the absence of caffeine led to a rapid down-regulation of $p27^{Kip1}$, but not $p21^{Cip1}$, levels (Fig. 1D, lane 2–6). However, in the presence of caffeine, $p21^{Cip1}$ levels also rapidly declined (Fig. 1D, cf. lanes 7–11 and 2–6). These results demonstrate that cell cycle re-entry of serum-starved TKO-Bcl2 MEFs was hampered by the DDR, which is indicative of the presence of DNA damage. We also noticed that treatment with caffeine accelerated cell cycle re-entry, but apparently did not result in progression to G1 phase, as, after 24 h, only a few cells with a 2n DNA content were present, in contrast to restimulation with 10% serum only (Fig. 1B, 24 h panels). This may indicate that, in the presence of caffeine, cells entered mitosis with a high amount of DNA damage that impeded proper mitosis and/or cytokinesis.

DNA damage in mitogen-deprived TKO-Bcl2 MEFs

Nuclear foci that are positive for both γ-H2AX and Rad51, a protein involved in homologous recombination by promoting strand invasion (Branzei and Foiani 2008), are indicative of the presence of DSBs (Paull et al. 2000). Figure 2A shows that such foci were present in mitogen-deprived TKO-Bcl2 MEFs, but were absent in TKO-Bcl2 MEFs cultured in the presence of 10% FCS, as well as in wild-type MEFs cultured in the presence or absence of 10% FCS. The percentage of TKO-Bcl2 MEFs carrying more than five γ-H2AX/Rad51 foci gradually increased upon serum deprivation to reach 60% after 7 d of mitogen deprivation (Fig. 2B).

We also assessed the presence of γ-H2AX/Rad51 foci in cells lacking pRB and p107, since these cells only partially arrested in G2 upon mitogen withdrawal (Supplemental Fig. S2A; Foijer et al. 2005), and loss of these two Rb proteins strongly stimulated development of retinoblastomas and other tumors in mice (Dannenberg et al. 2004). In mitogen-starved $Rb^{-/-}p107^{-/-}$ MEFs, both $p27^{Kip1}$ and $p21^{Cip1}$ protein levels were up-regulated

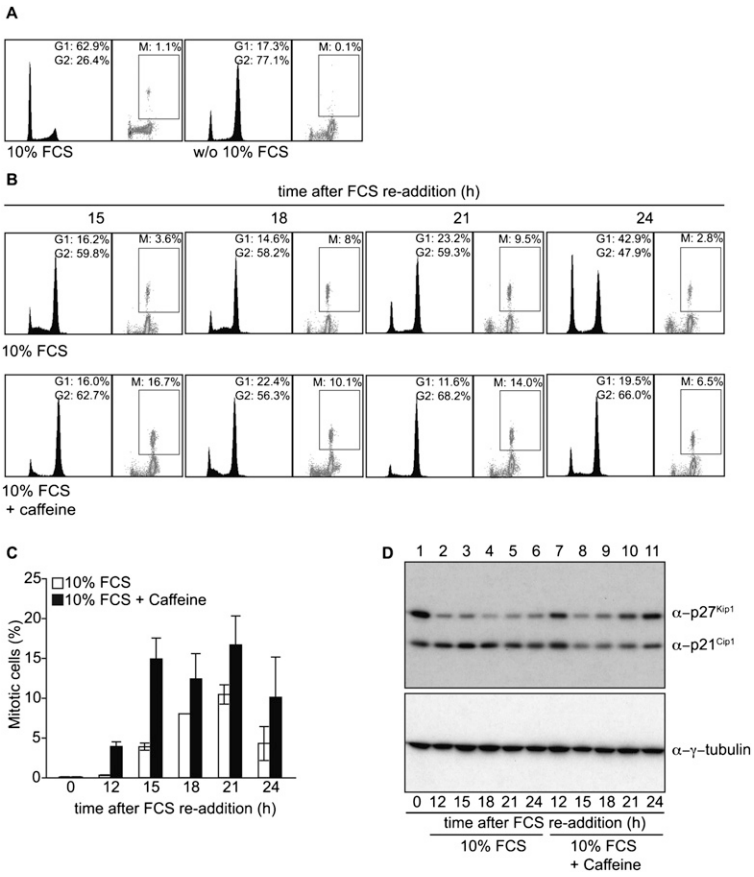

Figure 1. Inhibition of the DDR results in accelerated cell cycle re-entry of G2-arrested TKO-Bcl2 MEFs after serum readdition. (*A*,*B*) Cell cycle distribution and percentage of mitotic cells as measured by MPM2 positivity in TKO-Bcl2 MEFs cultured in the presence or absence (w/o) of 10% FCS (for 7 d) (*A*), and in serum-starved TKO-Bcl2 MEF cultures restimulated with 10% FCS for 15, 18, 21, and 24 h in the presence (*bottom* part) or absence (*top* part) of caffeine (*B*). (*C*) Percentage of mitotic cells in TKO-Bcl2 MEFs at different time points after serum readdition in either the presence (black bars) or absence (white bars) of caffeine. Graph represents average values of two independent experiments; error bars show standard deviations. (*D*) $p27^{Kip1}$ and $p21^{Cip1}$ protein levels in TKO-Bcl2 MEFs at different time points after serum readdition in either the presence (lanes *7–11*) or absence (lanes *2–6*) of caffeine. Anti-γ-tubulin was used as loading control.

(Supplemental Fig. S2B), and the number of cells positive for γ-H2AX/Rad51 foci corresponded to the number of cells arrested in G2 (Supplemental Fig. S2C,D).

Rad51 is expressed during late G1, S, and G2 phase of the cell cycle in murine cells (Yamamoto et al. 1996), and might therefore be a poor indicator of DSBs in early G1. To confirm the presence of DSBs in G2-arrested TKO-Bcl2 MEFs and their absence in G1-arrested wild-type MEFs (Fig. 2E), we assessed the presence of DSBs by performing neutral comet assays (Olive and Banath 2006). Comets could readily be detected in mitogen-deprived TKO-Bcl2 MEFs, while they were absent in TKO-Bcl2 MEFs cultured in the presence of 10% FCS and in wild-type Bcl2 MEFs cultured in the presence or absence of 10% FCS (Fig. 2C). Figure 2D shows that the mean tail moment, a quantitative indicator for the presence of DSBs, was significantly increased in mitogen-deprived TKO-Bcl2 MEFs, but not in mitogen-deprived wild-type Bcl2 MEFs. In contrast, when TKO-Bcl2 MEFs and wild-type Bcl2 MEFs were exposed to ionizing radiation (20 Gy), both cell types showed comets with comparable tail moments (Fig. 2C,D).

Thus, lack of pocket protein activity in combination with mitogen deprivation resulted in the formation of DSBs. Since wild-type MEFs did not contain DSBs and arrested in the G1 phase of the cell cycle upon mitogen withdrawal (Fig. 2E), these results indicate that the progression through an unscheduled S phase might be the cause of DSB formation.

Serum-restimulated TKO-Bcl2 MEFs re-entered the cell cycle with DNA damage

To examine whether cell cycle re-entry upon serum readdition was accompanied by DNA repair, we quantified the percentage of TKO-Bcl2 MEFs containing more than five γ-H2AX/Rad51 foci during incubation following serum readdition (Fig. 3B). Twenty-one hours after serum readdition, the number of cells containing γ-H2AX/Rad51 foci had decreased more than twofold, suggesting that repair had occurred. However, at 15 h, the number of cells carrying more than five foci had not yet decreased, while at this time the first cells had started to enter mitosis (Fig. 3A).

Since it has been shown previously that Rb deficiency resulted in a less stringent G2 arrest in response to DNA-damaging agents (Jackson et al. 2005; Eguchi et al. 2007), it could be possible that serum-restimulated TKO-Bcl2 MEFs re-entered the cell cycle with unrepaired DSBs. This was already suggested by the persistent elevated levels of $p21^{Cip1}$ in serum-restimulated TKO-Bcl2 MEFs (Fig. 1C, lanes 1–6) that were progressing into mitosis (Fig. 3A). To examine this further, we followed serum-restimulated TKO-Bcl2 MEFs by time-lapse microscopy. As a readout for DSBs, we monitored the presence of foci containing 53BP1, a mediator protein recruited to DSBs (Schultz et al. 2000). To this aim, a fusion protein of 53BP1 and GFP was expressed in TKO-Bcl2 MEFs. Expression of 53BP1-GFP did not interfere with mitotic entry of G2-arrested TKO-Bcl2

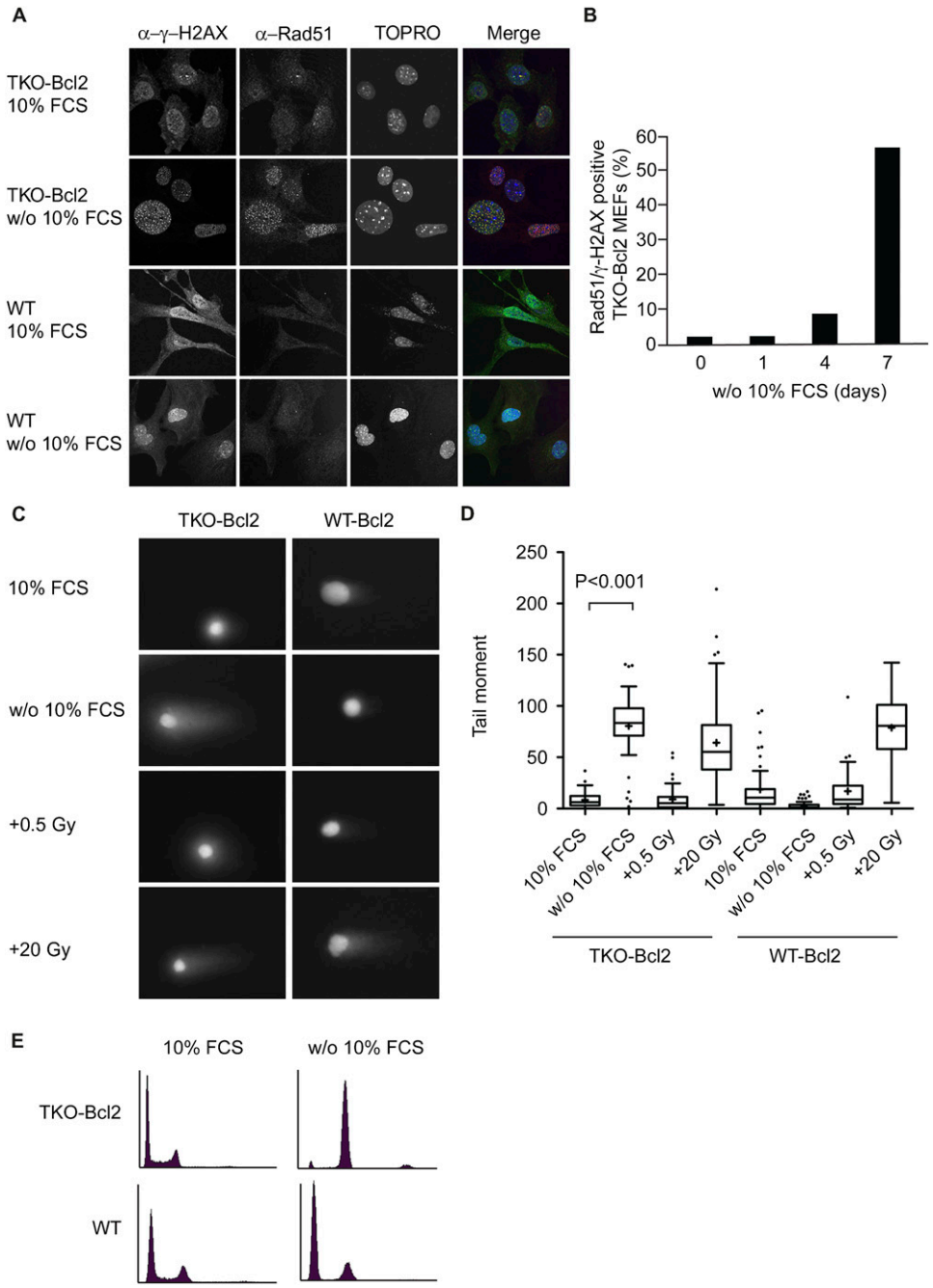

Figure 2. Serum-deprived TKO-Bcl2 MEFs contain DSBs. (*A*) Immunofluorescent images of TKO-Bcl2 and wild-type MEFs cultured in the presence or absence of 10% FCS (for 7 d) to detect γ-H2AX and Rad51 foci. DNA was labeled with TOPRO-3. In the merge picture, DNA is blue, γ-H2AX is green, Rad51 is red, and colocalization of γ-H2AX and Rad51 is seen as yellow foci. (*B*) Quantification of γ-H2AX/Rad51 focus formation in TKO-Bcl2 MEFs cultured without 10% FCS for 1, 4, and 7 d. Cells were considered positive when they contained five or more superimposed γ-H2AX and Rad51 foci. At least 100 cells were counted for each condition. (*C*) Representative comets of nuclei of TKO-Bcl2 and wild-type Bcl2 MEFs stained with propidium iodide cultured in the presence or absence of 10% FCS (for 7 d). Cells exposed to 0.5 or 20 Gy of γ-irradiation served as controls. (*D*) Tail moments obtained from TKO-Bcl2 and wild-type Bcl2 MEFs cultured in the presence (untreated or γ-irradiated with 0.5 or 20 Gy) or absence of 10% FCS (for 7 d). Box plots represent interquartile ranges, horizontal bars denote the median, plus (+) indicates the mean value, and points indicate outliers. For each condition, 50 cells were analyzed using the CASP software. (*E*) Cell cycle distribution as determined by propidium iodide staining of TKO-Bcl2 and wild-type MEFs cultured in the presence or absence of 10% FCS (for 7 d).

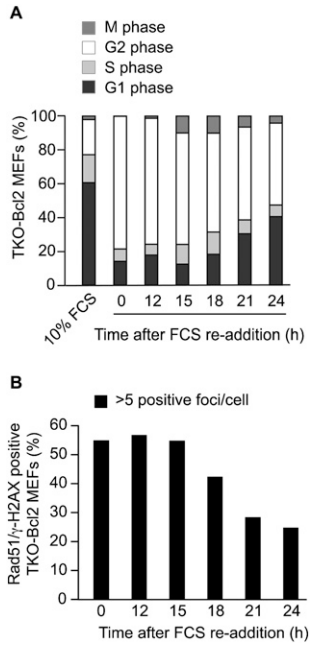

Figure 3. γ-H2AX/Rad51 foci partially dissolve when serum-restimulated TKO-Bcl2 MEFs re-enter the cell cycle. (*A*) Cell cycle distribution and percentage of mitotic cells in TKO-Bcl2 MEF cultures at different time points after FCS readdition. The percentages depicted in this graph represent five independent experiments. (*B*) Quantification of γ-H2AX/Rad51 foci in TKO-Bcl2 MEFs after FCS readdition. Cells were considered positive when they contained five or more foci positive for both γ-H2AX and Rad51. At least 100 cells were counted for each condition.

MEFs after serum readdition (Supplemental Fig. S3), nor did it result in the formation of aggregates in cycling cells that could be misinterpreted as DNA damage foci (Fig. 4B). Figure 4A shows two mitogen-deprived TKO-Bcl2 MEFs that still contained numerous 53BP1-GFP foci at 21 h after serum readdition (marked with + and ^). Eventually, these cells progressed into mitosis (27.5 and 31.5 h after serum readdition, respectively), with a clear decrease in the number of 53BP1-GFP foci. Nevertheless, one daughter cell still harbored some 53BP1-GFP foci after cytokinesis (Fig. 4A, marked with +, 36 h after FCS readdition, top cell). This indicates that not all of the DSBs in this cell were completely repaired before mitotic entry. Fifty-eight percent (30 out of 52) of the TKO-Bcl2 + 53BP1-GFP MEFs that we were able to follow for several hours before mitotic entry contained 53BP1-GFP foci. Strikingly, 53% (25 out of 47) of the cells that we could examine after cellular division still had 53BP1-GFP foci, although the number of foci was clearly reduced as illustrated in Figure 4A (data not shown). Thus, serum-restimulated TKO-Bcl2 MEFs re-entered the cell cycle in the presence of DNA damage foci indicative of remaining DSBs.

Chromosome abnormalities

To examine the presence of DNA damage in mitogen-deprived TKO-Bcl2 MEFs that had re-entered the cell cycle after serum readdition, we screened for chromosomal abnormalities in metaphase spreads from cells that were harvested 21 h after serum readdition. TKO-Bcl2 MEFs and wild-type MEFs hardly contained break events when they had always been cultured in the presence of 10% FCS (Fig. 5A). In contrast, in serum-deprived TKO-Bcl2 MEFs that were restimulated to enter mitosis, numerous chromatid breaks were present (Fig. 5B,F, indicated by arrows). Chromatid breaks were hardly observed in serum-starved and serum-restimulated wild-type MEFs (Fig. 5B,E), once more suggesting that progression through an aberrant S phase in the absence of mitogens resulted in chromosomal abnormalities.

In addition to chromatid breakages, we also observed defects in centromeric sister chromatid cohesion, as evidenced by a railroad track appearance of chromosomes (Fig. 5F, indicated by arrowheads). Figure 5D illustrates that, in 90% of serum-restimulated TKO-Bcl2 MEFs, >10 metaphase chromosomes no longer showed the typical tight centromeric cohesion. This is in sharp contrast to serum-restimulated wild-type MEFs (Fig. 5D,E), as well as TKO-Bcl2 and wild-type MEFs cultured in the presence of 10% FCS continuously (Fig. 5C), wherein the majority of cells did not show signs of loss of centromeric sister chromatid cohesion.

Sister chromatid cohesion is established during S phase by the cohesin complex (Peters et al. 2008). We determined whether inappropriate entry into S phase under growth-restricting conditions resulted in defects in cohesin loading. Supplemental Figure S4A shows that the levels of chromatin-associated Rad21, a subunit of the cohesin complex, did not differ between cells cultured in the presence or absence of 10% FCS, suggesting that the loading was not defective. This corresponds to the study by Manning et al. (2010) showing that compromised sister chromatid cohesion in pRB-depleted cells was not caused by loss of chromatin-associated cohesin complexes. Apart from loading defects, it is possible that the cohesin complex was removed prematurely during mitogen readdition. To exclude this, we assessed whether cohesion defects were already present in G2-arrested TKO-Bcl2 MEFs before serum restimulation. To this aim, G2-arrested cells were treated with Calyculin A, which induces premature chromosome condensation and thus allows the visualization of chromosomes in G2 (Gotoh 2009). Similar to metaphase spreads from restimulated TKO-Bcl2 MEFs, chromosome spreads from G2-arrested cells showed chromosome breaks and loss of centromeric cohesion (Supplemental Fig. S4B). Thus, although the cohesin complex was loaded properly onto the chromatin, the defects in sister chromatid cohesion were already present in G2-arrested cells, suggesting they had occurred in the preceeding S phase.

Genomic instability

We observed previously that proliferating cell cultures could be obtained from serum-restimulated TKO-Bcl2 MEFs (Foijer et al. 2005). To investigate whether the numerous chromatid breaks and losses of centromeric cohesion in serum-stimulated TKO-Bcl2 MEFs gave rise to numerical or structural chromosomal alterations in this proliferating population, we generated 13 clones from

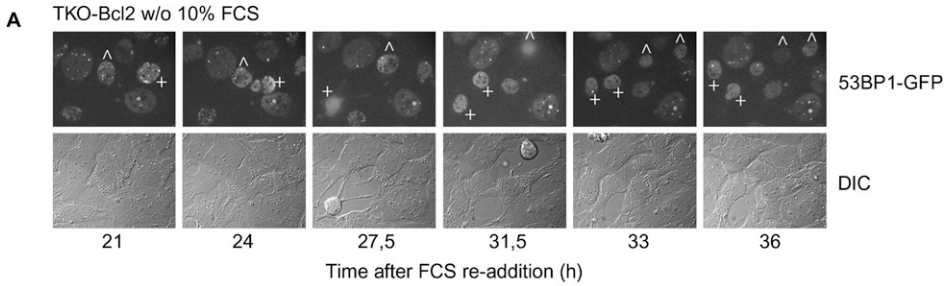

C

Before M-phase	No 53 BP1 foci	22
	53 BP1 foci	30
	out of position	11
After M-phase	No 53 BP1 foci	22
	53 BP1 foci	25 *
	out of position	13
	dead/no division	3

* less compared to before M-phase

Figure 4. Live-cell imaging of TKO-Bcl2 MEFs expressing 53BP1-GFP. (*A*) 53BP1-GFP foci in mitogen-deprived TKO-Bcl2 MEFs restimulated with serum for the indicated times. TKO-Bcl2 MEFs that entered mitosis are marked with ^ and +. (*B*) 53BP1-GFP-positive TKO-Bcl2 MEFs (marked with asterisk [*]) going through mitosis cultured in the presence of 10% FCS continuously. (*C*) Quantification of the number of serum-restimulated TKO-Bcl2 MEFs containing 53BP1-GFP foci before and after M phase.

single cells. These clones were analyzed by array-based comparative genomic hybridization (aCGH) for CNAs. Eight of the 13 clones were obtained from single cells that were in mitosis 21 h after serum readdition (Table 1, clones 6–13 [without 10% FCS]). In five of these clones, we detected CNAs. Since these restimulated cells had entered M phase relatively late (Fig. 1B), and thus may be more severely damaged, we might have overestimated the presence of chromosomal aberrations in the entire proliferating population. Therefore, we also analyzed five clones generated from single cells out of the whole cell population obtained 48 h after serum readdition (Table 1, clones 1–5 [without 10% FCS]). In this case, severely damaged cells may have been counterselected, as nondamaged or moderately damaged cells may have entered the cell cycle earlier and dominated the population. Nevertheless, also in this case, we observed chromosome aberrations in one clone that had gained chromosome 15 and lost part of chromosome 12 (Fig. 6A). Thus, in 46% of all clones derived from serum-starved TKO-Bcl2 MEFs, we found CNAs. In contrast, we detected CNAs in only 16% of cell clones derived from TKO-Bcl2 MEFs that had always been cultured in the presence of 10% FCS (Table 1, clones 1–11 [10% FCS]).

To investigate whether, in addition to numerical alterations, structural aberrations had also occurred, we applied multiplex FISH (M-FISH) to 11 TKO-Bcl2 clones derived from single cells (Table 1, clones 1–3 [10% FCS] and clones 1–8 [without 10% FCS]; Jentsch et al. 2001). Strikingly, we only rarely found evidence for translocations. One clone showed an unbalanced translocation, t(12;15), in 100% of the analyzed cells (Fig. 6C), corresponding to the gain of chromosome 15 and partial loss of chromosome 12 detected by aCGH in this clone (Fig. 6A). The M-FISH analyses generally confirmed the gains and losses detected by aCGH. However, by M-FISH, we detected CNAs that were absent in the aCGH profiles, but most of the time, these aberrations were present in the minority of metaphase spreads (Table 1).

Interestingly, unlike TKO-Bcl2 MEFs cultured in 10% FCS continuously (Dannenberg et al. 2000; Vormer et al. 2008), one of these genetically altered cell clones was able to form colonies in soft agar upon expression of Ras^{V12} (Supplemental Fig. S5). This shows that this clone had progressed toward a more transformed phenotype. Taken together, these analyses show that a temporary period of mitogen deprivation in pocket protein-deficient MEFs resulted in genetically altered cell clones, mainly manifested

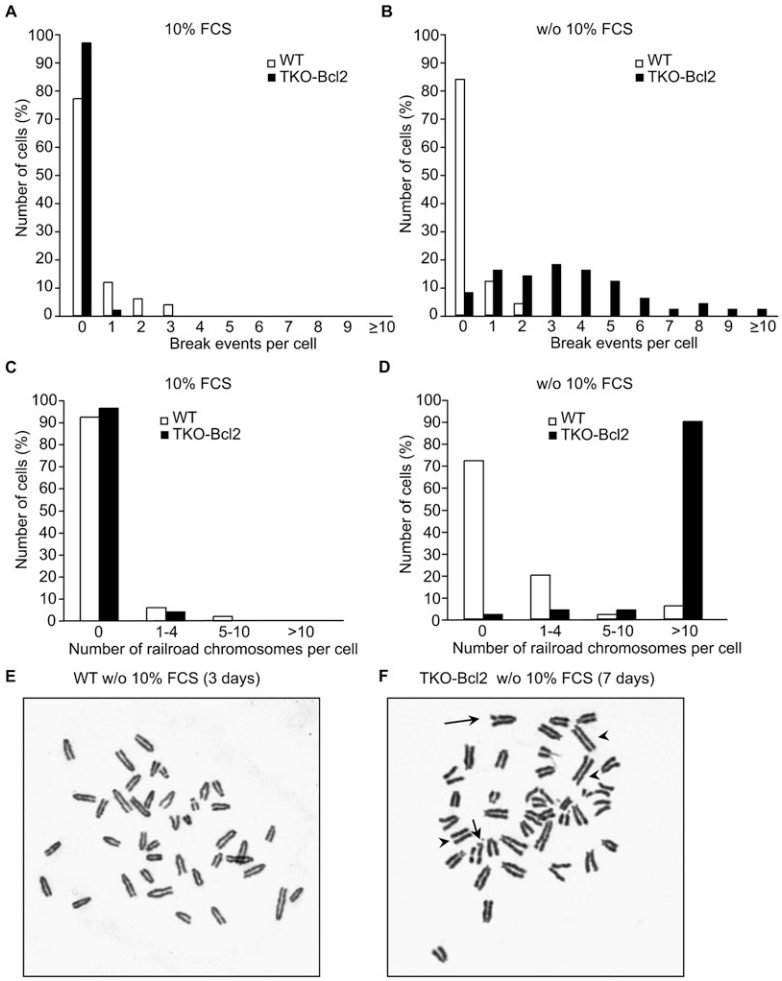

Figure 5. Serum deprivation of TKO-Bcl2 MEFs results in chromosomal aberrations. (*A*,*B*) Quantification of chromosomal breakage events in proliferating TKO-Bcl2 MEFs and wild-type MEFs (*A*) and serum-restimulated (21 h) TKO-Bcl2 MEFs after 7 d of mitogen deprivation and serum-restimulated wild-type MEFs after 3 d of mitogen deprivation (*B*). (*C*,*D*) Quantification of loss of centromeric cohesion in proliferating TKO-Bcl2 MEFs and wild-type MEFs (*C*) and serum-restimulated (21 h) TKO-Bcl2 MEFs after 7 d of mitogen deprivation and serum-restimulated wild-type MEFs after 3 d of mitogen deprivation (*D*). (*A–D*) Per condition, 50 metaphases were evaluated. (*E*,*F*) Chromosome spread of serum-restimulated wild-type MEFs after 3 d of mitogen deprivation (*E*) and serum-restimulated (21 h) TKO-Bcl2 MEFs after 7 d of mitogen deprivation (*F*). Arrows indicate chromatid breaks, and arrowheads indicate railroad chromosomes.

by chromosome gains or losses that might promote tumorigenesis.

Discussion

We demonstrate here that mitogen deprivation in MEFs devoid of G1/S control (TKO-Bcl2 and $Rb^{-/-}p107^{-/-}$ MEFs) resulted in the formation of DSBs. These DSBs are sensed by the DDR, leading to the accumulation of the CKI $p21^{Cip1}$. We showed previously that up-regulation of $p21^{Cip1}$ in mitogen-deprived TKO-Bcl2 MEFs contributed to a sustained G2 arrest by inhibiting the activity of Cyclin A–CDK2 as well as Cyclin B–CDK1 complexes (Foijer et al. 2005). However, G2 arrest in mitogen-deprived TKO-Bcl2 MEFs did not rely solely on the DDR: Treatment of mitogen-deprived TKO-Bcl2 MEFs with caffeine (without the addition of 10% FCS) was not sufficient to force cells into mitosis (Foijer et al. 2005), although it did reduce $p21^{Cip1}$ levels (Fig. 1D). The reason is that the CKI $p27^{Kip1}$ is also induced upon mitogen deprivation due to reduced PI-3 kinase activity (Foijer et al. 2008). Thus, $p21^{Cip1}$ and $p27^{Kip1}$ both contribute to G2 arrest, although they are induced by different mechanisms.

Our study also revealed another type of chromosomal abnormality in mitogen-starved TKO-Bcl2 MEFs: loss of sister chromatid cohesion. Interestingly, compromised centromeric sister chromatid cohesion was also observed upon pRB depletion in RPE-1 cells, and this promoted merotelic attachments (A Manning and N Dyson, pers. comm.).

Importantly, we detected only DSBs and cohesion defects in TKO-Bcl2 MEFs that were cultured in the absence but not in the presence of mitogenic stimuli. This contradicts previous findings. Normal human keratinocytes expressing HPV-16 E7 contained increased numbers of γ-H2AX foci (Duensing and Munger 2002), and *Rb* inactivation or expression of HPV E7 in normal human fibroblasts resulted in the formation of DSBs (Pickering and Kowalik 2006). Besides the difference in cell type, in these studies, methods were used to acutely down-regulate the Rb pathway, contrary to our study where the three pocket proteins were constitutively absent. The latter may have allowed for up-regulation of compensatory pathways to counteract DSB formation in the presence of serum. Furthermore, it is uncertain whether the culture conditions were optimal in all cases. Thus, culture stress due to suboptimal culture conditions might result in DNA damage in cells deprived of Rb protein activity.

A question that remains is how culture stress, effectuated by serum deprivation, in TKO-Bcl2 MEFs resulted in the formation of DSBs and cohesion defects. Mitogen

Table 1. *Summary of the numerical and structural aberrations detected by CGH and M-FISH in single-cell clones derived from TKO-Bcl2 MEFs cultured in the presence or absence of 10% FCS*

		M-FISH	
Clone	CGH	Most spreads	Some spreads
1 (10% FCS)	No changes		Loss chr. 6 Transl. (6;6) Transl. (2;6)
2 (10% FCS)	No changes		Loss chr. 11, 14 Gain chr. 17
3 (10% FCS)	No changes		Gain chr. 3, 5, 8, Y Loss chr. 12, 14
4 (10% FCS)	No changes	n.d.	n.d.
5 (10% FCS)	No changes	n.d.	n.d.
6 (10% FCS)	No changes	n.d.	n.d.
7 (10% FCS)	No changes	n.d.	n.d.
8 (10% FCS)	No changes	n.d.	n.d.
9 (10% FCS)	Loss chr. 1 (part) Gain chr. 8, 11	n.d.	n.d.
10 (10% FCS)	No changes	n.d.	n.d.
11 (10% FCS)	Gain chr. 10 (part)	n.d.	n.d.
1 (without 10% FCS)	No changes		Gain chr. 6, 7, 8, 12, 15 Loss chr. 14
2 (without 10% FCS)	No changes		Loss chr. 12, Y
3 (without 10% FCS)	No changes		Gain chr. 7, 8, 12, Y Loss chr. Y
4 (without 10% FCS)	No changes		Gain chr. 4 Transl. (8;11)
5 (without 10% FCS)	Loss chr. 12 (part) Gain chr. 15	Transl. (12; 15)	Loss chr. 3
6 (without 10% FCS)	Loss chr. 7	Loss chr. Y	Loss chr. 4, 19 Gain chr. 5, 17
7 (without 10% FCS)	Loss chr. 8, 11	Loss chr. 7, 8, 11	Loss chr. 1, 9, 12, 13, 14, 16, 18, Y Gain chr. 2, 6, 7, 13, 15, 16, 19 Transl. (6;7),(8;17)
8 (without 10% FCS)	Loss chr. 1, 7, 12 Mini chr. 5	Loss chr. 1, 7, 8, 12, 14	Loss chr. 3, 11, 13, 17, Y Gain chr. 2, 4, 6, 9, 10, 11, 13, 15, 17, 19, Y
9 (without 10% FCS)	Loss chr. 14, 17	n.d.	n.d.
10 (without 10% FCS)	No changes	n.d.	n.d.
11 (without 10% FCS)	No changes	n.d.	n.d.
12 (without 10% FCS)	No changes	n.d.	n.d.
13 (without 10% FCS)	Loss chr. 14	n.d.	n.d.

(Most spreads) More than 50% of the metaphase spreads; (some spreads) less than 50% of the metaphase spreads; (chr.) chromosome; (Transl.) translocation; (n.d.) not determined.

deprivation did not induce these abnormalities in wild-type MEFs that arrested in G1. Mitogen-deprived TKO-Bcl2 MEFs did enter S phase because of the absence of G1/S control, suggesting that chromosome aberrations resulted from replication stress. Previously, we showed that the accumulation of $p21^{Cip1}$ and $p27^{Kip1}$ in serum-starved TKO-Bcl2 MEFs caused inhibition of Cyclin A- and Cyclin B-associated kinase activities (Foijer et al. 2005). Cyclin A has been implicated in S-phase progression by activating the DNA polymerase δ-dependent elongation machinery (Bashir et al. 2000), and blocking Cyclin A activity inhibited progression through S phase (Yam et al. 2002). Thus, the reduced Cyclin A-associated kinase activity in serum-deprived TKO-Bcl2 MEFs might cause perturbations in S-phase progression, causing replication fork stalling and collapse, eventually leading to DSBs (Helleday et al. 2008). Interestingly, a DDR has been observed previously upon activation of various oncogenes, and has been ascribed to stalling and collapse of replication forks (Bartkova et al. 2006; Di Micco et al. 2006; Halazonetis et al. 2008). Furthermore, the establishment of sister chromatid cohesion occurs at replication forks, and it has been suggested that this might also be disturbed during replication stress (Peters et al. 2008). Indirectly, defects in sister chromatid cohesion could compromise the repair of DSBs (Watrin and Peters 2006) occurring after mitogen deprivation.

We observed that serum-restimulated TKO-Bcl2 MEFs repaired DSBs before entering mitosis, since the number of cells containing γ-H2AX/Rad51 foci decreased, as well as the number of 53BP1-GFP foci in single cells that were followed by time-lapse microscopy. Furthermore, cell cycle re-entry of these cells was at least partially dependent on down-regulation of the activity of the DDR, since treatment with caffeine resulted in an accelerated cell cycle re-entry. Strikingly, though, the majority of restimulated cells ended up in mitosis, with several remaining chromatid

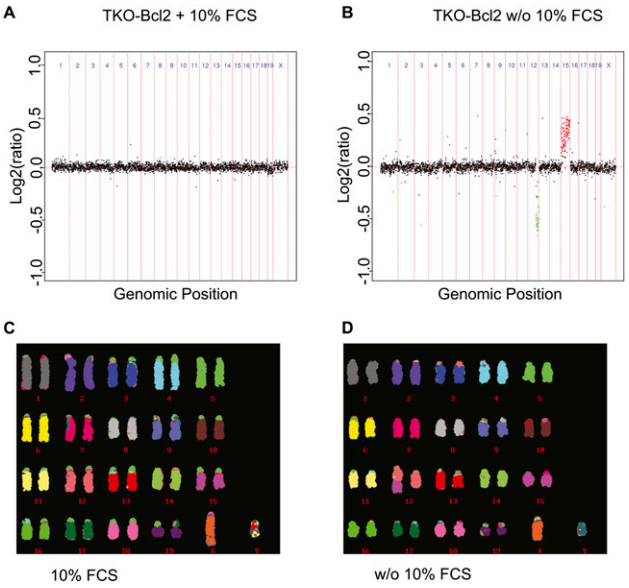

Figure 6. Single-cell clones derived from serum-restimulated TKO-Bcl2 MEFs contain CNAs. (*A*,*B*) aCGH profiles of clones derived from TKO-Bcl2 cell cultured in 10% FCS continuously (*A*) or serum-restimulated TKO-Bcl2 cell (plated 48 h after serum readdition) (*B*). Log_2 hybridization ratios are plotted for 2803 BAC clones, represented on the CGH microarray, at their genomic position. Red dots represent amplifications >0, and green dots represent deletions <0 (Rosetta error model; $P < 0.01$). (*C*,*D*) M-FISH analysis of cells used in *A* and *B*, respectively.

breaks per cell. This may indicate that, once the $p27^{Kip1}$ protein levels were reduced by serum readdition, the DDR, resulting in high levels of $p21^{Cip1}$, was not sufficiently stringent to keep DNA damage-containing TKO-Bcl2 MEFs in G2.

The low stringency of the DDR-induced G2 arrest may be a direct consequence of loss of the Rb pathway. Indeed, several studies have shown that cells lacking Rb function had a less prominent G2 arrest in response to DNA damage due to an inability to down-regulate genes that promote G2/M progression (Hernando et al. 2004; Jackson et al. 2005; Eguchi et al. 2007). Additionally, it has been reported that a normally functioning G2/M checkpoint is not that stringent, since cells with 10–20 DSBs in G2 are allowed to enter mitosis (Deckbar et al. 2007). However, the implications of a negligent G2/M checkpoint in damaged cells for genome integrity in descendent cells are not well known.

We now show that mitotic chromosomal abnormalities, like chromatid breaks and cohesion defects, can be detrimental for genomic integrity, since we obtained proliferating cell clones of serum-starved and serum-restimulated TKO-Bcl2 MEFs that contained CNAs. How chromatid breaks and cohesion defects contribute to CNAs is not entirely clear. Previous work showed that uncorrected merotelic attachments can give rise to lagging chromosomes during anaphase, eventually causing missegregation (Cimini et al. 2001). Thus, it is likely that the defects in centromeric cohesion in serum-restimulated TKO-Bcl2 MEFs resulted in the genetic alterations we observed in descendent cell clones. In line with this, it was demonstrated recently that chromatid cohesion defects resulted in chromosomal instability in human cells, and were detected in a subset of human cancers (Barber et al. 2008).

Human retinoblastomas are genetically unstable (Dimaras et al. 2008), but this phenomenon has not been linked thus far to defects in DNA repair. An intriguing question is whether loss of G1/S control in combination with inappropriate growth conditions could induce genomic instability and promote oncogenic transformation in vivo.

Materials and methods

Cell culture and constructs

MEFs were isolated from chimeric embryos as described previously (Dannenberg et al. 2000), and were cultured in GMEM (Invitrogen-GIBCO) supplemented with 10% FCS, 0.1 mM nonessential amino acids (Invitrogen-GIBCO), 1 mM sodium pyruvate (Invitrogen-GIBCO), 100 μl/mL penicillin, 100 μg/mL streptomycin (Invitrogen-GIBCO), and 0.1 mM β-mercaptoethanol (Merck). Bcl2-expressing MEFs were generated as described previously (Foijer et al. 2005). The retroviral vector encoding 53BP1-GFP has been described (van Vugt et al. 2010); pBABE-Ras^{V12} was kindly provided by T. Brummelkamp. TKO-Bcl2 + 53BP1-GFP MEFs and Ras^{V12}-expressing cells were obtained using the same transfection/infection protocol (Foijer et al. 2005). For serum starvation experiments, cells were trypsinized and allowed to attach in the presence of serum for 4 h. Subsequently, cells were washed with PBS and supplemented with serum-free medium. For serum restimulation experiments, serum-free medium was replaced after 7 d by complete medium. In the case of caffeine or UCN-01 treatment, cells were incubated with 5 mM caffeine (Sigma) or 300 nM UCN-01 in serum-containing medium. UCN-01 was generously provided by Kyowa Hakko Kogyo Co.

Immunoblots and antibodies

Cells were harvested and subsequently lysed for 30 min in ELB (150 mM NaCl, 50 mM Hepes at pH 7.5, 5 mM EDTA, 0.1% NP-40) containing protease inhibitors (Complete; Roche). Protein concentrations were measured using the Bradford assay (Bio-Rad) or BCA protein assay kit (Pierce). For chromatin isolation, cells were harvested and subsequently lysed for 30 min in ELB^+ (150 mM NaCl, 50 mM Hepes at pH 7.5, 5 mM EDTA, 0.5% NP-40, 6% glycerol) containing protease inhibitors (Complete; Roche), sodium orthovanadat, sodium fluoride, and glycerol 2-phosphate disodiumsalthydrate. After centrifugation (3 min at 5000 rpm), the supernatant was taken as soluble fraction, and the pellet was washed three times and used as chromatin fraction.

The primary antibodies used were rabbit polyclonal p21 (C19; Santa Cruz Biotechnology), mouse monoclonal p27 (BD Transduction Laboratory), goat CDK4 (C22; Santa Cruz Biotechnology), rabbit polyclonal Histone H2B (Upstate Biotechnologies), and γ-tubulin (GTU-88; Sigma). Secondary antibodies used were HRP-conjugated goat anti-mouse and HRP-conjugated goat anti-rabbit (Dako).

Immunofluorescence

For immunofluorescence stainings, cells were cultured on cover slides, washed with PBS, and fixed for 5 min using 4% paraformaldehyde (Merck). Cells were permeabilized by 0.1% Triton

X-100 (Sigma) in PBS for 5 min. Subsequently, cells were washed three times using staining buffer (0.15% glycine [Merck], 0.5% bovine serum albumine [BSA; Sigma] in PBS), and were incubated for 60 min at room temperature in staining buffer. Cells were incubated for 4 h and 1 h with primary and secondary antibodies, respectively. Bleaching was prevented by Vectashield (Vector Laboratories). The primary antibodies used were rabbit polyclonal Rad51 (a gift from Professsor Dr. Roland Kanaar) and mouse monoclonal phosphorylated H2AX (Upstate Biotechnologies) in 1:2500 and 1:100 dilutions in staining buffer, respectively. Secondary antibodies used were Alexa 488-labeled chicken anti-mouse and Alexa 568-labeled goat anti-rabbit antibodies (Molecular Probes), and these were used in a 1:200 dilution in staining buffer. DNA was stained using To-Pro3 dye (Molecular Probes).

Comet assay

Neutral comet assays were performed as described by Olive and Banath (2006). Briefly, 8×10^3 cells were diluted in 0.4 mL of PBS and were added to 1.2 mL of 1% low-gelling-temperature agarose (Sigma). Subsequently, the cell suspension was transferred onto precoated slides (Menzel-Gläser). Cell lysis was performed in neutral lysis solution (2% sarkosyl, 0.5 M Na_2EDTA, 0.5 mg/mL proteinase K) at pH 8.0 overnight at 37°C. Slides were washed three times with neutral rinse and electrophoresis buffer (90 mM Tris, 90 mM boric acid, 2 mM Na_2EDTA) at pH 8.5, and electrophoresis was performed in neutral rinse and electrophoresis buffer for 25 min at 20 V. Nuclei were stained with 2.5 μg/mL propidium iodide (Invitrogen) in distilled water for 20 min. Pictures of individual cells were taken with a Zeiss AxioObserver Z1 inverted microscope equipped with a cooled Hamamatsu ORCA AG black-and-white CCD camera, and were analyzed with CASP software (http://www.casp.of.pl). The *P*-value was measured using one-way ANOVA (nonparametric Kruskal-Wallis test).

Time-lapse microscopy

For time-lapse microscopy experiments, cells were plated on 35-mm glass-bottom culture dishes (Willco dishes). Mitogen-deprived cells were followed from 1 h after serum readdition until 48 h later. For live imaging, dishes were transferred to a heated stage (37°C) on a Zeiss Axiovert 200M microscope equipped with a 0.55 numerical aperture (N.A.) condensor and a 40× Achroplan objective (N.A., 0.60). Twelve-bit DIC (digital image contrast) images (100-msec exposure) and fluorescent images (50-msec exposure) were captured every 5 min using a Photometrics Coolsnap HQ CCD camera set at gain 1.0 (Scientific) and appropriate filter cubes (Chroma Technology Corp.) to select specific fluorescence. Images were processed using Metamorph software (Universal Imaging).

Flow cytometry

After fixation in ice-cold 70% ethanol, cells were stained with mouse anti-MPM2 antibody (Upstate Biotechnologies) for 1 h in a 1:200 dilution. The secondary antibody used was Alexa 488-labeled chicken anti-mouse (Molecular Probes) in a 1:200 dilution. Subsequently, cells were counterstained with propidium iodide diluted in PBS containing RNase. Finally, the percentage of mitotic cells (MPM2 positivity) and the cell cycle distribution (propidium iodide) of the cells were determined by flow cytometry, using Cell Quest software (BD Bioscience).

Chromosome spreads

For chromosome spreads, mitogen-deprived MEFs were serum-restimulated for 21 h, and were treated with 0.2 μg/mL colcemid (Sigma) during the last 45 min to trap cells in mitosis or were treated with only 50 nM Calyculin A (Invitrogen) for 30 min. Cells were forced to swell using 75 mM KCl for 10 min, and were subsequently fixed by a 3:1 mixture of methanol and acetic acid. Prior to light microscopy, cells were spread on microscope slides. Per condition, 50 spreads were analyzed for chromosome breakage events and loss of centromeric cohesion. We scored the number of chromatid breaks as well as chromatid interchanges as described in Joenje et al. (1981). Depending on its complexity, a chromatid interchange was counted as one or two breaks. The numbers of chromatid breaks derived from chromatid interchanges per total number of break events per culture were as follows: wild type + 10% FCS: two out of 18; TKO-Bcl2 + 10% FCS: zero out of one; wild type without 10% FCS: four out of eight; TKO-Bcl2 without 10% FCS: 14 out of 172. We did not find chromosome break events.

Genomic DNA isolation, fragmentation, labeling, and BAC array hybridization

Genomic DNA from test and control TKO MEFs was extracted and purified with the DNeasy blood and tissue kit (Qiagen). Subsequently, DNA was fragmented using the Bioruptor (Diagenode). Fragment sizes were checked on a 1% agarose gel (100–600 base pairs [bp]). Test and reference DNA were labeled with the Kreatech ULS array CGH labeling kit (Kreatech). Test DNA was derived from single-cell clones of serum-restimulated TKO-Bcl2 MEFs (plated either 48 h after serum readdition [whole population] or 21 h after serum readdition [mitotic cells only]) and single-cell clones of TKO-Bcl2 MEFs cultured in the presence of 10% FCS continuously. As reference DNA, we used genomic DNA isolated from TKO-Bcl2 MEFs cultured in the presence of 10% FCS continuously. The fluorescently labeled DNA was hybridized on a 3K mouse BAC microarray as described previously (Chung et al. 2004). The Rosetta error model was used to calculate weighted averages and statistical confidence levels. All values with *P*-values <0.01 were considered to represent significant CNAs.

M-FISH

Single-cell clones were cultured and treated with 0.02 μg/mL colcemid (Sigma) for 2 h to obtain metaphase-arrested cells. Cells were subjected to an osmotic shock (75 mM KCl) for 10 min and fixed in 3:1 methanol:acetic acid. Prior to hybridization, cells were dropped on microscope slides, aged overnight, and treated with 0.01% pepsin (Sigma) for 5 min. Slides were baked for 1 h at 65°C before denaturation at 63°C in 70% formamide/2× SSC, and then were dehydrated through an ethanol series (70%, 90%, and 100%). Individual mouse paints were prepared using flow-sorted mouse chromosomes as described previously (Jentsch et al. 2001). The "mouse paint mix" was prepared using whole-chromosome-specific paints labeled with a different combination of four fluorochromes (Cy5, Texas Red, Cy3, and FITC) and one hapten (Biotin). Each chromosome in the mix was labeled with a unique combination of three or fewer fluorochomes, except for chromosome Y, which was labeled with all five. Mouse paint was denatured for 10 min at 65°C, and 7 μl of paint was applied to each slide. Slides were incubated for 48 h at 37°C, washed in 50% formamide/2× SSC at 43°C, and then incubated with one layer of Streptavidin Dylight 680 conjugate (Thermo Fisher Scientific) for biotin. Slides were counterstained with 10 μl of 4,6,diamidino-2-phenylindole (DAPI) counterstain in anti-fade. Images of metaphase spreads were captured using a Leica 5000DM epifluorescent microscope equipped with narrow bandpass filter sets for DAPI, FITC, Cy3, Texas Red, Cy5, and

Cy5.5, and a cooled CCD camera. For each metaphase spread, six images were captured using filter combinations specific for each of the five fluorochromes and DAPI. A minimum of 10 metaphases were captured from each cell line and were analyzed using Leica CW 4000 CytoFISH software.

Soft agar assay

Soft agar assays were performed as described previously (Vormer et al. 2008). Briefly, 6×10^4 MEFs were suspended in 0.35% soft agar solution, plated on one well of a six-well plate, and incubated for 3 wk at 37°C. Pictures were taken using a non-phase-contrast lens (2.5× magnification) and assembled using Axiovision 4.5.

Acknowledgments

We thank R. Kanaar for rabbit polyclonal Rad51 antibody, Kyowa Hakko Kogyo Co. for UCN-01, and B. Fu for the M-FISH reagents. We thank L. Oomen and L. Brocks for help with the microscopical visualization of the comets, W. van Zon for help with time-lapse microscopy, and W. Brugman for help with aCGH. We are grateful to N. Carter, T. Vormer, S. Bakker, and M. Aarts for fruitful discussions and critically reading the manuscript. This work was supported by the Dutch Cancer Society (NKI 2007-3790) and the Wellcome Trust (grant no. WT077008).

References

Amato A, Lentini L, Schillaci T, Iovino F, Di Leonardo A. 2009. RNAi mediated acute depletion of retinoblastoma protein (pRb) promotes aneuploidy in human primary cells via micronuclei formation. *BMC Cell Biol* **10:** 79. doi: 10.1186/1471-2121-10-79.

Barber TD, McManus K, Yuen KW, Reis M, Parmigiani G, Shen D, Barrett I, Nouhi Y, Spencer F, Markowitz S, et al. 2008. Chromatid cohesion defects may underlie chromosome instability in human colorectal cancers. *Proc Natl Acad Sci* **105:** 3443–3448.

Bartkova J, Rezaei N, Liontos M, Karakaidos P, Kletsas D, Issaeva N, Vassiliou LV, Kolettas E, Niforou K, Zoumpourlis VC, et al. 2006. Oncogene-induced senescence is part of the tumorigenesis barrier imposed by DNA damage checkpoints. *Nature* **444:** 633–637.

Bashir T, Horlein R, Rommelaere J, Willwand K. 2000. Cyclin A activates the DNA polymerase δ-dependent elongation machinery in vitro: A parvovirus DNA replication model. *Proc Natl Acad Sci* **97:** 5522–5527.

Bosco EE, Mayhew CN, Hennigan RF, Sage J, Jacks T, Knudsen ES. 2004. RB signaling prevents replication-dependent DNA double-strand breaks following genotoxic insult. *Nucleic Acids Res* **32:** 25–34.

Branzei D, Foiani M. 2008. Regulation of DNA repair throughout the cell cycle. *Nat Rev Mol Cell Biol* **9:** 297–308.

Burkhart DL, Sage J. 2008. Cellular mechanisms of tumour suppression by the retinoblastoma gene. *Nat Rev Cancer* **8:** 671–682.

Chung YJ, Jonkers J, Kitson H, Fiegler H, Humphray S, Scott C, Hunt S, Yu Y, Nishijima I, Velds A, et al. 2004. A whole-genome mouse BAC microarray with 1-Mb resolution for analysis of DNA copy number changes by array comparative genomic hybridization. *Genome Res* **14:** 188–196.

Cimini D, Howell B, Maddox P, Khodjakov A, Degrassi F, Salmon ED. 2001. Merotelic kinetochore orientation is a major mechanism of aneuploidy in mitotic mammalian tissue cells. *J Cell Biol* **153:** 517–527.

Corson TW, Gallie BL. 2007. One hit, two hits, three hits, more? Genomic changes in the development of retinoblastoma. *Genes Chromosomes Cancer* **46:** 617–634.

Dannenberg JH, van Rossum A, Schuijff L, te Riele H. 2000. Ablation of the retinoblastoma gene family deregulates G(1) control causing immortalization and increased cell turnover under growth-restricting conditions. *Genes Dev* **14:** 3051–3064.

Dannenberg JH, Schuijff L, Dekker M, van der Valk M, te Riele H. 2004. Tissue-specific tumor suppressor activity of retinoblastoma gene homologs p107 and p130. *Genes Dev* **18:** 2952–2962.

Deckbar D, Birraux J, Krempler A, Tchouandong L, Beucher A, Walker S, Stiff T, Jeggo P, Lobrich M. 2007. Chromosome breakage after G2 checkpoint release. *J Cell Biol* **176:** 749–755.

Dimaras H, Khetan V, Halliday W, Orlic M, Prigoda NL, Piovesan B, Marrano P, Corson TW, Eagle RC Jr, Squire JA, et al. 2008. Loss of RB1 induces non-proliferative retinoma: Increasing genomic instability correlates with progression to retinoblastoma. *Hum Mol Genet* **17:** 1363–1372.

Di Micco R, Fumagalli M, Cicalese A, Piccinin S, Gasparini P, Luise C, Schurra C, Garre M, Nuciforo PG, Bensimon A, et al. 2006. Oncogene-induced senescence is a DNA damage response triggered by DNA hyper-replication. *Nature* **444:** 638–642.

Doorbar J. 2006. Molecular biology of human papillomavirus infection and cervical cancer. *Clin Sci (Lond)* **110:** 525–541.

Duensing S, Munger K. 2002. The human papillomavirus type 16 E6 and E7 oncoproteins independently induce numerical and structural chromosome instability. *Cancer Res* **62:** 7075–7082.

Eguchi T, Takaki T, Itadani H, Kotani H. 2007. RB silencing compromises the DNA damage-induced G2/M checkpoint and causes deregulated expression of the ECT2 oncogene. *Oncogene* **26:** 509–520.

Foijer F, Wolthuis RM, Doodeman V, Medema RH, te Riele H. 2005. Mitogen requirement for cell cycle progression in the absence of pocket protein activity. *Cancer Cell* **8:** 455–466.

Foijer F, Simonis M, van Vliet M, Wessels L, Kerkhoven R, Sorger PK, Te Riele H. 2008. Oncogenic pathways impinging on the G2-restriction point. *Oncogene* **27:** 1142–1154.

Gonzalo S, Garcia-Cao M, Fraga MF, Schotta G, Peters AH, Cotter SE, Eguia R, Dean DC, Esteller M, Jenuwein T, et al. 2005. Role of the RB1 family in stabilizing histone methylation at constitutive heterochromatin. *Nat Cell Biol* **7:** 420–428.

Gotoh E. 2009. Drug-induced premature chromosome condensation (PCC) protocols: Cytogenetic approaches in mitotic chromosome and interphase chromatin. *Methods Mol Biol* **523:** 83–92.

Graves PR, Yu L, Schwarz JK, Gales J, Sausville EA, O'Connor PM, Piwnica-Worms H. 2000. The Chk1 protein kinase and the Cdc25C regulatory pathways are targets of the anticancer agent UCN-01. *J Biol Chem* **275:** 5600–5605.

Halazonetis TD, Gorgoulis VG, Bartek J. 2008. An oncogene-induced DNA damage model for cancer development. *Science* **319:** 1352–1355.

Harper JW, Elledge SJ. 2007. The DNA damage response: Ten years after. *Mol Cell* **28:** 739–745.

Helleday T, Petermann E, Lundin C, Hodgson B, Sharma RA. 2008. DNA repair pathways as targets for cancer therapy. *Nat Rev Cancer* **8:** 193–204.

Hernando E, Nahle Z, Juan G, Diaz-Rodriguez E, Alaminos M, Hemann M, Michel L, Mittal V, Gerald W, Benezra R, et al. 2004. Rb inactivation promotes genomic instability by

uncoupling cell cycle progression from mitotic control. *Nature* **430:** 797–802.

Iovino F, Lentini L, Amato A, Di Leonardo A. 2006. RB acute loss induces centrosome amplification and aneuploidy in murine primary fibroblasts. *Mol Cancer* **5:** 38. doi: 10.1186/1476-4598-5-38.

Jackson MW, Agarwal MK, Yang J, Bruss P, Uchiumi T, Agarwal ML, Stark GR, Taylor WR. 2005. p130/p107/p105Rb-dependent transcriptional repression during DNA-damage-induced cell-cycle exit at G2. *J Cell Sci* **118:** 1821–1832.

Jentsch I, Adler ID, Carter NP, Speicher MR. 2001. Karyotyping mouse chromosomes by multiplex-FISH (M-FISH). *Chromosome Res* **9:** 211–214.

Joenje H, Arwert F, Eriksson AW, de Koning H, Oostra AB. 1981. Oxygen-dependence of chromosomal aberrations in Fanconi's anaemia. *Nature* **290:** 142–143.

Knudsen KE, Booth D, Naderi S, Sever-Chroneos Z, Fribourg AF, Hunton IC, Feramisco JR, Wang JY, Knudsen ES. 2000. RB-dependent S-phase response to DNA damage. *Mol Cell Biol* **20:** 7751–7763.

Malumbres M, Barbacid M. 2001. To cycle or not to cycle: A critical decision in cancer. *Nat Rev Cancer* **1:** 222–231.

Manning AL, Longworth MS, Dyson NJ. 2010. Loss of pRB causes centromere dysfunction and chromosomal instability. *Genes Dev* (this issue). doi: 10.1101/gad.1917310.

Marx J. 2002. Debate surges over the origins of genomic defects in cancer. *Science* **297:** 544–546.

Mayhew CN, Bosco EE, Fox SR, Okaya T, Tarapore P, Schwemberger SJ, Babcock GF, Lentsch AB, Fukasawa K, Knudsen ES. 2005. Liver-specific pRB loss results in ectopic cell cycle entry and aberrant ploidy. *Cancer Res* **65:** 4568–4577.

Medema RH, Kops GJ, Bos JL, Burgering BM. 2000. AFX-like Forkhead transcription factors mediate cell-cycle regulation by Ras and PKB through p27kip1. *Nature* **404:** 782–787.

Olive PL, Banath JP. 2006. The comet assay: A method to measure DNA damage in individual cells. *Nat Protoc* **1:** 23–29.

Paull TT, Rogakou EP, Yamazaki V, Kirchgessner CU, Gellert M, Bonner WM. 2000. A critical role for histone H2AX in recruitment of repair factors to nuclear foci after DNA damage. *Curr Biol* **10:** 886–895.

Perez-Ordonez B, Beauchemin M, Jordan RC. 2006. Molecular biology of squamous cell carcinoma of the head and neck. *J Clin Pathol* **59:** 445–453.

Peters JM, Tedeschi A, Schmitz J. 2008. The cohesin complex and its roles in chromosome biology. *Genes Dev* **22:** 3089–3114.

Pickering MT, Kowalik TF. 2006. Rb inactivation leads to E2F1-mediated DNA double-strand break accumulation. *Oncogene* **25:** 746–755.

Sage J, Mulligan GJ, Attardi LD, Miller A, Chen S, Williams B, Theodorou E, Jacks T. 2000. Targeted disruption of the three Rb-related genes leads to loss of G(1) control and immortalization. *Genes Dev* **14:** 3037–3050.

Sarkaria JN, Busby EC, Tibbetts RS, Roos P, Taya Y, Karnitz LM, Abraham RT. 1999. Inhibition of ATM and ATR kinase activities by the radiosensitizing agent, caffeine. *Cancer Res* **59:** 4375–4382.

Schultz LB, Chehab NH, Malikzay A, Halazonetis TD. 2000. p53 binding protein 1 (53BP1) is an early participant in the cellular response to DNA double-strand breaks. *J Cell Biol* **151:** 1381–1390.

Srinivasan SV, Mayhew CN, Schwemberger S, Zagorski W, Knudsen ES. 2007. RB loss promotes aberrant ploidy by deregulating levels and activity of DNA replication factors. *J Biol Chem* **282:** 23867–23877.

van Vugt MA, Gardino AK, Linding R, Ostheimer GJ, Reinhardt HC, Ong SE, Tan CS, Miao H, Keezer SM, Li J, et al. 2010. A mitotic phosphorylation feedback network connects Cdk1, Plk1, 53BP1, and Chk2 to inactivate the G(2)/M DNA damage checkpoint. *PLoS Biol* **8:** e1000287. doi: 10.1371/journal.pbio.1000287.

Vormer TL, Foijer F, Wielders CL, te Riele H. 2008. Anchorage-independent growth of pocket protein-deficient murine fibroblasts requires bypass of G2 arrest and can be accomplished by expression of TBX2. *Mol Cell Biol* **28:** 7263–7273.

Watrin E, Peters JM. 2006. Cohesin and DNA damage repair. *Exp Cell Res* **312:** 2687–2693.

Yam CH, Fung TK, Poon RY. 2002. Cyclin A in cell cycle control and cancer. *Cell Mol Life Sci* **59:** 1317–1326.

Yamamoto A, Taki T, Yagi H, Habu T, Yoshida K, Yoshimura Y, Yamamoto K, Matsushiro A, Nishimune Y, Morita T. 1996. Cell cycle-dependent expression of the mouse Rad51 gene in proliferating cells. *Mol Gen Genet* **251:** 1–12.

Zheng L, Flesken-Nikitin A, Chen PL, Lee WH. 2002. Deficiency of retinoblastoma gene in mouse embryonic stem cells leads to genetic instability. *Cancer Res* **62:** 2498–2502.